PNAS RESEARCH ARTICLE | MEDICAL SCIENCES

Engineering an inducible leukemia-associated fusion protein enables large-scale ex vivo production of functional human phagocytes

Roland Windisch[a], Sarah Soliman[a], Adrian Hoffmann[b,c], Linping Chen-Wichmann[a], Anna Danese[d], Sebastian Vosberg[e,f,g,h], Jimena Bravo[i], Sebastian Lutz[a], Christian Kellner[a], Alexander Fischer[j], Claudia Gebhard[k], Enric Redondo Monte[e,f,g], Luise Hartmann[e,f,g], Stephanie Schneider[e,l,m], Fabian Beier[n], Carolin Dorothea Strobl[e,f,g], Oliver Weigert[e,f,g], Matthias Peipp[o], Michael Schündeln[p], Stefan H. Stricker[d], Michael Rehli[j,k], Jürgen Bernhagen[b,q], Andreas Humpe[a], Hannes Klump[r,s], Christian Brendel[t], Daniela S. Krause[i,u], Philipp A. Greif[e,f,g,1], and Christian Wichmann[a,1,2]

Affiliations are included on p. 11.

Edited by Nancy Speck, Raymond and Ruth Perelman School of Medicine at the University of Pennsylvania, Philadelphia, PA; received August 1, 2023; accepted March 20, 2024

Ex vivo expansion of human CD34+ hematopoietic stem and progenitor cells remains a challenge due to rapid differentiation after detachment from the bone marrow niche. In this study, we assessed the capacity of an inducible fusion protein to enable sustained ex vivo proliferation of hematopoietic precursors and their capacity to differentiate into functional phagocytes. We fused the coding sequences of an FK506-Binding Protein 12 (FKBP12)-derived destabilization domain (DD) to the myeloid/lymphoid lineage leukemia/eleven nineteen leukemia (MLL-ENL) fusion gene to generate the fusion protein DD-MLL-ENL and retrovirally expressed the protein switch in human CD34+ progenitors. Using Shield1, a chemical inhibitor of DD fusion protein degradation, we established large-scale and long-term expansion of late monocytic precursors. Upon Shield1 removal, the cells lost self-renewal capacity and spontaneously differentiated, even after 2.5 y of continuous ex vivo expansion. In the absence of Shield1, stimulation with IFN-γ, LPS, and GM-CSF triggered terminal differentiation. Gene expression analysis of the obtained phagocytes revealed marked similarity with naïve monocytes. In functional assays, the novel phagocytes migrated toward CCL2, attached to VCAM-1 under shear stress, produced reactive oxygen species, and engulfed bacterial particles, cellular particles, and apoptotic cells. Finally, we demonstrated Fcγ receptor recognition and phagocytosis of opsonized lymphoma cells in an antibody-dependent manner. Overall, we have established an engineered protein that, as a single factor, is useful for large-scale ex vivo production of human phagocytes. Such adjustable proteins have the potential to be applied as molecular tools to produce functional immune cells for experimental cell-based approaches.

CD34+ | human blood progenitors | macrophages | MLL1 | cellular differentiation

Significance

In this study, we demonstrated that an engineered inducible fusion protein expands human blood progenitors as a single factor and upon inactivation promotes differentiation to phagocytes. Altogether, we converted a leukemic fusion protein into a powerful protein switch for large-scale ex vivo production of functional human phagocytes able to adhere, migrate, clear apoptotic cells, and engulf both bacterial particles and opsonized lymphoma cells. Thus, generated phagocytes are fully functional rendering the principle a promising approach in producing immune cells in large-scale.

Hematopoietic stem cells give rise to all functional blood cell types, including immune cells, and therefore are routinely used for transplantation during treatment of cancer and immune system disorders. Compared with blood cell donations, ex vivo-generated effector blood cells could be produced with distinct antigen profiles and characteristics. As long-term ex vivo expansion of hematopoietic stem and progenitor cells (HSPCs) is highly challenging, novel methods are required to conduct efficient ex vivo progenitor cell expansion. However, propagation of HSPCs requires the complex 3D interaction framework of the hematopoietic niche within the bone marrow (1–3). After precursor cells detach from this niche, the cells rapidly lose self-renewal capacities and differentiate. This phenomenon renders it difficult to expand and produce blood cells ex vivo in relevant numbers, e.g., for in vitro cell-based experiments with rare hematopoietic progenitor populations. Therefore, reliable cell biological procedures are required for large-scale expansion and consecutive differentiation into fully functional blood cells.

The generation of induced pluripotent stem cells (iPSCs) is a novel technique that involves the overexpression of at least three different transcription factors that together convert somatic cells into pluripotent stem cells capable of differentiating into various human tissues (4). Although this new technology offers multiple options for cell production, the highly complex and time-consuming nature of the method poses some disadvantages for the production of human blood cells. With respect to human CD34+ cell expansion, recent reports have suggested that a few chimeric fusion genes originally discovered in human

Author contributions: R.W., L.C.-W., C.K., C.B., D.S.K., P.A.G., and C.W. designed research; R.W., S. Soliman, A. Hoffmann, L.C.-W., J. Bravo, S.L., A.F., C.G., E.R.M., L.H., S. Schneider, and F.B. performed research; J. Bravo, C.K., C.D.S., O.W., M.P., M.R., J. Bernhagen, and D.S.K. contributed new reagents/analytic tools; R.W., S. Soliman, A. Hoffmann, L.C.-W., A.D., S.V., J. Bravo, A.F., F.B., M.S., S.H.S., J. Bernhagen, A. Humpe, P.A.G., and C.W. analyzed data; and R.W., H.K., P.A.G., and C.W. wrote the paper.

The authors declare no competing interest.

This article is a PNAS Direct Submission.

[1]P.A.G. and C.W. contributed equally to this work.

[2]To whom correspondence may be addressed. Email: christian.wichmann@med.uni-muenchen.de.

This article contains supporting information online at https://www.pnas.org/lookup/suppl/doi:10.1073/pnas.2312499121/-/DCSupplemental.

Published June 10, 2024.

leukemia cells confer remarkable ex vivo progenitor cell expansion capacity, including fusion genes typically found in acute myeloid leukemia such as RUNX1/ETO, MLL-fusions, and NUP98-HOX fusions (5–14). These genes encode for chimeric proteins that assemble epigenetic regulators at the promoter sequence of relevant target genes. They modify physiological gene expression patterns, thereby conferring extensive self-renewal properties to blood progenitor cells. Importantly, these chimeric genes on their own are sufficient to induce large-scale ex vivo expansion of human CD34+ blood progenitor cells in liquid cultures containing cytokines without the supportive bone marrow niche cells. Apart from genetic manipulation to achieve self-renewal (e.g., ectopic expression of transcription factors), there has been remarkable progress in the development of drug-based hematopoietic stem cell self-renewal, for example by the epigenetic modifier UM171 (a pyrimido-indole derivative) or StemRegenin1, an aryl hydrocarbon receptor (AHR) antagonist (15–19). For mouse HSCs, a culture system in which albumin was replaced for polyvinyl alcohol, and which contains high concentrations of thrombopoietin and low concentrations of stem-cell factor on fibronectin-coated plates has been shown to mediate significant ex vivo HSC expansion (20).

In the current study, we utilize the fusion protein MLL-ENL (ME), found in human pediatric and adult ALL and AML patients, to generate a protein switch (21). MLL is a critical transcription factor involved in early blood development and is frequently found fused to various partner genes (22). The ENL portion of MLL-ENL assembles a functionally new multiprotein complex leading to a disturbed MLL1 target gene expression pattern (e.g., upregulation of *HOX* genes) consecutively enhancing self-renewal programs and establishing a differentiation blockage (23). MLL and ENL are highly structured proteins that contain multiple domains for DNA binding, oligomerization, recruitment of transcriptionally active proteins, and several other functions (24–26). In AML, MLL chimeric genes have been recurrently associated with monocytic leukemia (27). Notably, inducible expression of MLL-ENL in murine blood progenitor cells has been shown to induce granulocyte-like cells with segmented nuclei in ex vivo cultures, although the studies lacked granulocyte function data (28, 29).

Here, we describe a unique approach to generate functional human phagocytes using CD34+ HSPCs and applying a regulable system involving the MLL-ENL fusion protein fused to a tunable protein stabilization domain. We demonstrate that oncogenic expansion capacity can be utilized to produce unlimited numbers of precursor cells, which upon inactivation of MLL-ENL can be fully differentiated into human effector immune cells with complete reversion of the transformed phenotype to a normal cell physiology state. We illustrate the concept of engineering leukemia-associated inducible fusion proteins conferring sustained and powerful self-renewal properties to human blood progenitors, which upon inactivation of the inducible factor differentiate into fully functional blood cells. Such generated phagocytes may be used for modeling infection biology approaches, wound healing studies, and targeted anticancer chimeric antigen receptor (CAR) phagocytes for experimental, preclinical cell therapy approaches (30). This concept represents a proof-of-principle that may be particularly important for the development of techniques to generate functional human blood cells.

Results

An Engineered MLL-ENL Protein Switch (DD-ME) Confers Rapid Ex Vivo Selection and Expansion of Human Hematopoietic Progenitor Cells. To establish long-term and large-scale expansion of immature human hematopoietic progenitor cells, we utilized the extensive expansion-mediating capacity of the chimeric fusion protein MLL-ENL found in pediatric and adult leukemia. By fusing an FKBP12-derived destabilization domain (DD) together with a short poly-linker to the N terminus of MLL-ENL (DD-ME), we rendered the protein activity adjustable, as rapid proteasomal degradation of DD fusion proteins was shown in the absence of the DD-specific ligand Shield1 (31). This adjustable fusion protein was engineered to confer expansion of hematopoietic progenitor cells and subsequent differentiation by removing Shield1 (Fig. 1*A*). The chimeric fusion gene ME is frequently found in AML with monocytic maturation (27, 32), linking ME target genes to monopoiesis. Indeed, gene ontology analysis (33–35) of ME target genes (36) revealed the enrichment of genes associated with negative regulation of monocytic differentiation (Fig. 1*B*). For stable expression of ME, we utilized a standard retroviral expression vector with eGFP as a marker gene (Fig. 1*C*). In fact, when Shield1 was administered every other day, DD-ME gave rise to complete selection of transduced cells within 30 to 40 d, even with initial transduction rates of <5%, constituting a homogeneous population of small and undifferentiated cells as assessed via flow cytometry forward and side scatter profiling (Fig. 1 *D* and *E*). The rising slope of the curve indicates immediate growth advantage upon transduction compared to untransduced cells in the same culture (*SI Appendix*, Fig. S1 *A* and *B*). Initial selection worked best in medium containing IL-3, IL-6, SCF, TPO, Flt3-L, and GM-CSF. For further expansion, IL-3 and Flt3-L were sufficient for the continuous growth of previously selected precursor cells (*SI Appendix*, Fig. S1 *C–E*). Selection and expansion could not be achieved with media associated with lymphoid, erythroid, or thrombocytic cell culture (*SI Appendix*, Fig. S2 *A* and *B*). Upon Shield1 depletion, DD-ME disappeared as measured using intracellular staining against the particular destabilization domain (Fig. 1*F*). We also observed the downregulation of *HOXA9*, a critical direct target gene of ME (29) (Fig. 1*G*). However, overexpression of various *HOX* genes was not sufficient to provoke the depicted growth advantage (*SI Appendix*, Fig. S3*A*). Furthermore, when peripheral blood mononuclear cells (PBMCs) were used instead of human CD34+ precursor cells, DD-ME-induced expansion was not observed, thereby indicating that the immortalizing activity of the fusion protein was only active in progenitor cells (Fig. 1*H*).

DD-ME-Triggered Cell Proliferation and Self-Renewal Depend Entirely on the Presence of Shield1. To demonstrate the continuous dependency of DD-ME selected and expanded progenitors on Shield1, we removed the ligand during ex vivo expansion at various time points (Fig. 2*A*). We observed complete precursor cell dependency on a permanent supply of Shield1, even after 2.5 y of ex vivo growth. Upon Shield1 removal, the cells stopped proliferating, dramatically lost self-renewal capacity, and lacked colony formation capacity in semisolid medium after subsequent terminal differentiation (Fig. 2*B*). To explore infrequent events, we escalated the input cell number; however, we did not detect any colonies in Shield1-deprived and differentiated cells (*SI Appendix*, Fig. S3*B*). Importantly, reapplication of Shield1 after 5 d of Shield1 deprivation did not reinduce proliferation (*SI Appendix*, Fig. S3*C*). These results suggest that the DD-ME progenitor cells represent late monocytic progenitors which is in line with RNA-seq data revealing a distinct variation between the DD-ME +Shield1 progenitor cells and adult bone-marrow and cord blood CD34+ cells (*SI Appendix*, Fig. S3*D*). Cell proliferation of DD-ME progenitors completely remained Shield1-dependent even under approximated bone marrow cellular environment settings by coculturing with both, stromal cell lines such as OP9 and HS-5, and human primary mesenchymal stem cell-derived spheroids (*SI Appendix*, Fig. S4 *A–C* and S5 *A* and *B*). Using medium with either 20% fetal calf serum

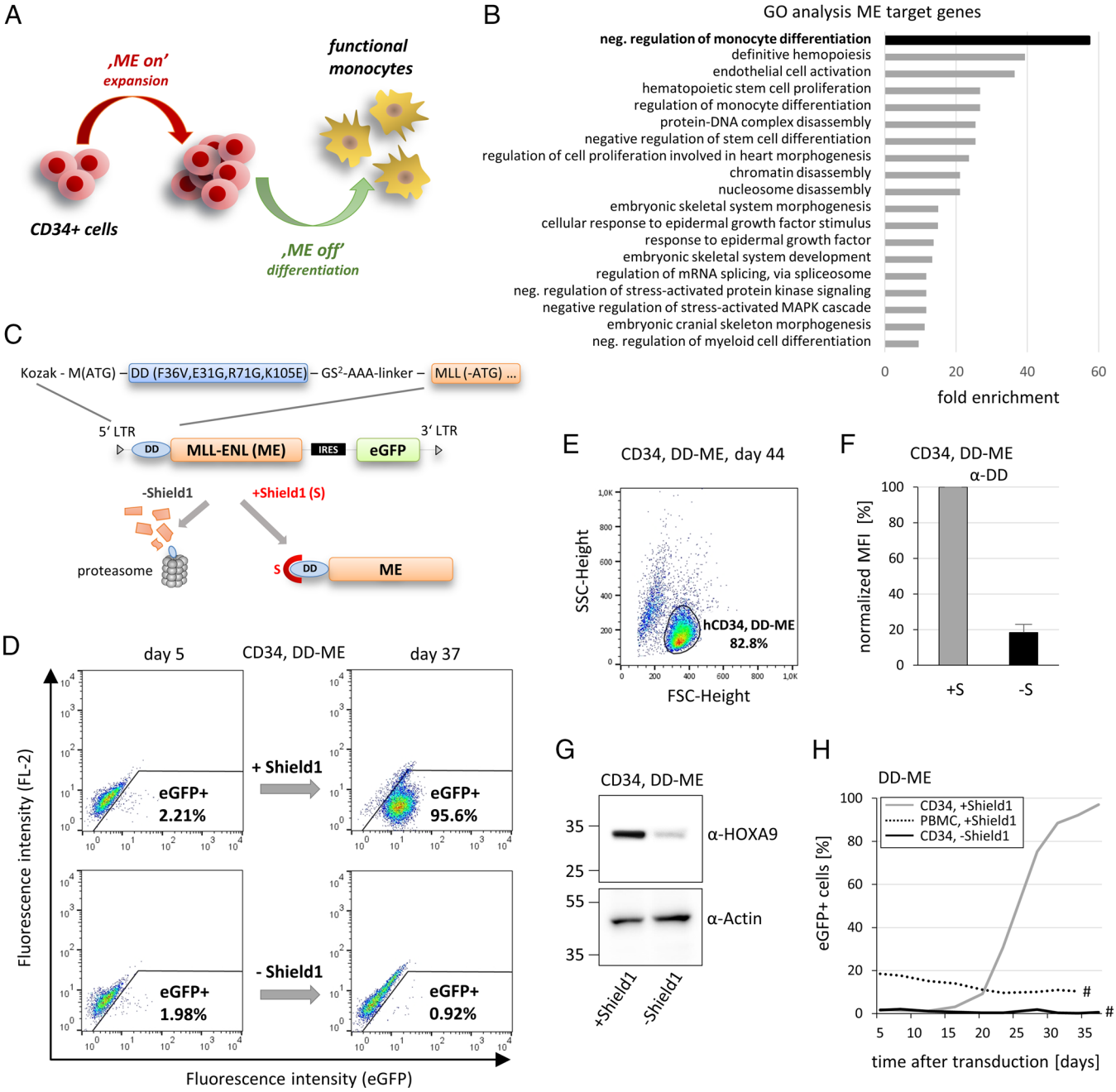

Fig. 1. Establishment of a protein switch for human hematopoietic stem and progenitor cell expansion using the MLL-ENL (ME) fusion gene and the Shield1 destabilization domain (DD). (*A*) Illustration of the procedure by which functional monocytes were derived from transduced and expanded human bone marrow CD34+ cells. (*B*) Gene ontology (GO) analysis of ME target genes (36) categorized by function (33–35). (*C*) A depiction of the retroviral vector containing ME fused to a DD destabilization domain (DD-ME). (*D*) Transduced CD34+ cells cultured in the presence of IL-3, IL-6, SCF, TPO, Flt3-L, and GM-CSF with or without Shield1 and analyzed for eGFP expression. (*E*) FSC/SSC profiles of DD-ME-expressing cells in the presence of Shield1 at day 44 posttransduction. (*F*) DD-ME signal intensity in the presence of Shield1 (+S) and after withdrawal of Shield1 (for 7 d) via intracellular staining. The data are presented as the mean plus the SD of three biological replicates. (*G*) Western blot analysis of HOXA9 expression using whole cell lysates of DD-ME-expressing cells before and after Shield1 removal. (*H*) Outgrowth of transduced, eGFP-expressing cells was determined via flow cytometry. #, terminally differentiated; FSC, forward scatter; SSC, side scatter.

(FCS) or 10% human serum, we observed massive cell expansion from 1×10^6 cells to 1.3×10^9 cells after 3 wk, which represents a 1,300-fold expansion with an average doubling time of 2.2 d (Fig. 2 *C* and *D*). The proliferation and differentiation characteristics of cells treated with FCS and human serum were comparable (*SI Appendix*, Fig. S6 *A–C*). Expanded precursor cells exhibited a normal karyotype and telomere length in a comparable range with human blood monocytes (37, 38). A trend toward a decrease in length after long-term culture and differentiation was observed. In addition, no difference in terms of telomere lengths was detected for cells cultivated with 10% human serum compared to 20% FCS-cultivated cells. Furthermore, the cells did not acquire copy number alterations and putative driver mutations as assessed by full exome sequencing. Mutations were found exclusively in transduced cells at MLL (KMT2A) loci, resulting from integration and retroviral overexpression of the MLL-ENL fusion. Retroviral integration site analysis of outgrown populations resulted in a similar oligo- to polyclonal pattern as recently described for MLL-AF9 ex vivo expanded human CD34+ cells (39) (*SI Appendix*, Fig. S7 *A–F*). Moreover, removal of cytokines and Shield1 did not result in clonal expansion during cell stress-selective pressure (Fig. 2*E*).

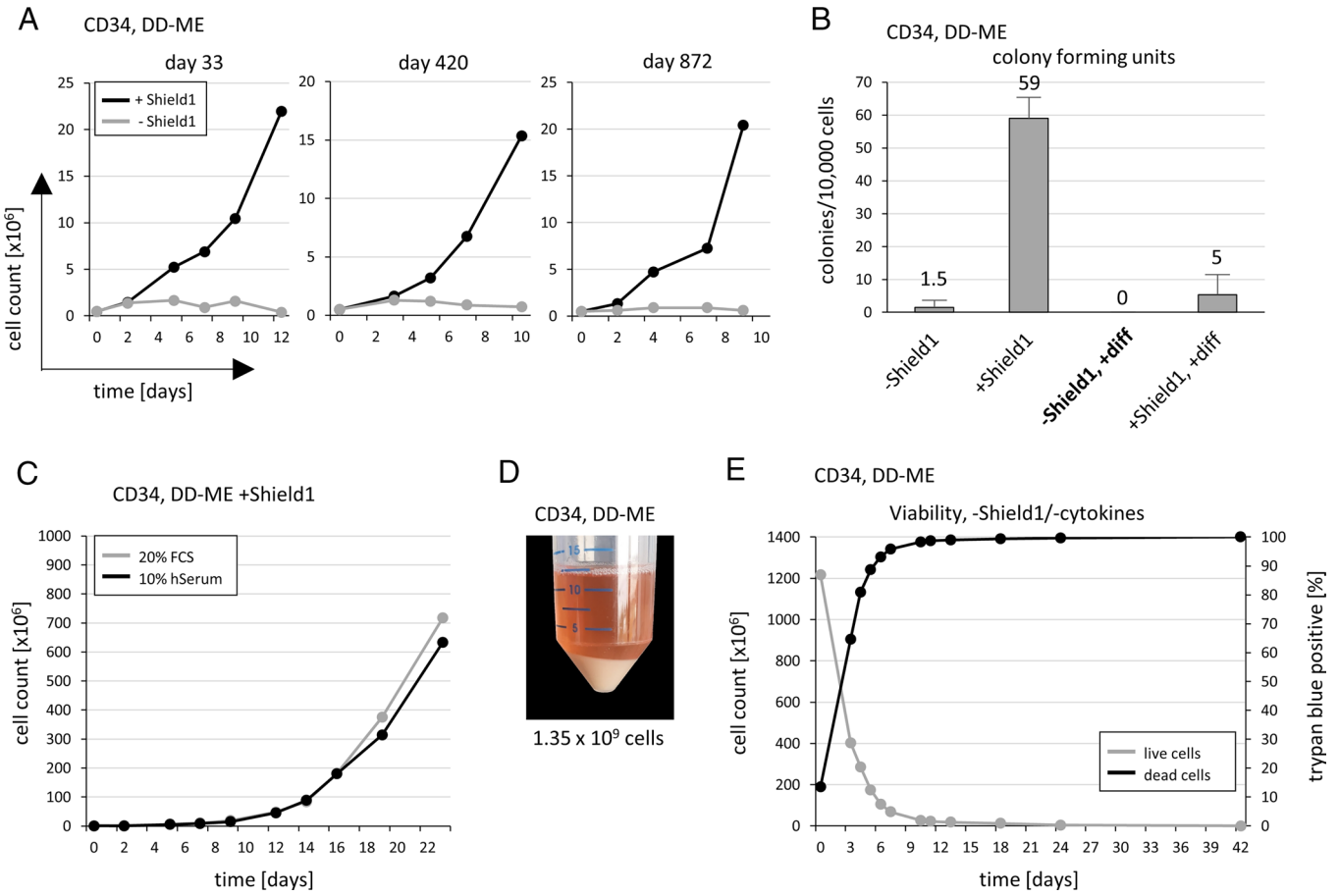

Fig. 2. Proliferation kinetics of DD-ME cells in the presence and absence of Shield1. (*A*) The growth curves of DD-ME-expressing cells with an initial cell count of 0.5×10^6 started at different time points after transduction with and without Shield1. (*B*) Colony-forming unit (CFU) assay with DD-ME expressing cells cultured in either complete or differentiation medium (10% FCS, GM-CSF, IFN-γ, LPS) with or without Shield1 for 7 d. The data are presented as the mean plus the SD of three biological replicates. (*C*) Expansion capacity of DD-ME cells in the presence of IL-3, Flt3-L, and Shield1 and supplemented with either FCS or human serum. (*D*) Image of 1.35×10^9 cells after 22 d of expansion (FCS and human serum samples combined). (*E*) Viability assay of DD-ME cells after withdrawal of IL-3, Flt3-L, and Shield1 to detect cytokine- and Shield1-independent single cell outgrowth.

DD-ME Expands Late Monocytic Precursor Cells and Shutdown of the Protein Switch Induces Monocytic Differentiation Including Fc and MHC Surface Receptor Upregulation. The DD-ME selected and expanded cells expressed CD14 and possessed an immature phenotype with a high nucleus to cytoplasm ratio. The progenitors showed low levels of leukocyte peroxidase and high levels of esterase staining, thus resembling late monocytic precursor cells (Fig. 3*A*). Six days after Shield1 removal, cultivated cells changed in size and granularity even more obvious in the presence of GM-CSF in combination with LPS and IFN-γ, and showed a shift in the nucleus to cytoplasm ratio (Fig. 3*B*). The resulting cells gained the ability to adhere to plastic surfaces showing an elongated morphology, which was more pronounced when the differentiation process was extended up to 14 d (Fig. 3*C*). To assess monocytic differentiation, we deprived the cells of Shield1 and cultivated the cells in medium containing various combinations of stimuli. Treatment with GM-CSF, IFN-γ, and LPS appeared most effective to produce highly viable macrophage-like cells (*SI Appendix*, Fig. S8*A*). Notably, Shield1 deprivation was necessary to yield well-defined cell differentiation (*SI Appendix*, Fig. S8*B*). In the presence of GM-CSF, IFN-γ, and LPS an average of 65% of DD-ME progenitor cells terminally differentiated within 12 d as assessed by live-cell imaging (*SI Appendix*, Fig. S9 *A* and *B*). Single cell RNA sequencing of DD-ME cells harvested at varying differentiation time points confirmed a uniform differentiation toward a single cell fate. During the differentiation course, the cells gradually up-regulated macrophage-associated markers resulting in the highest macrophage score for the fully differentiated, homogeneous cell population (Fig. 3*D* and *SI Appendix*, Fig. S10*A*). Accordingly, differentiated cells permanently exited the cell cycle and up-regulated markers such as CD14 and CD86 while down-regulating proliferation-related genes such as *MYB*, *BIRC5*, or *TOP2A* (*SI Appendix*, Fig. S10 *B–E*). Analyzing the macrophage-like characteristics of the differentiated cells via flow cytometry revealed upregulation of surface markers characteristic of both M1 and M2 macrophages. The M1 macrophage surface markers included the protein B7 molecules CD80 and CD86. We also detected CD163 expression, thereby indicating a mixed phenotype of both macrophage subtypes. Moreover, the differentiated cells displayed CD11b/Mac-1 expression and CD14 upregulation in accordance with the scRNA-sequencing results (Fig. 3*E* and *SI Appendix*, Fig. S11). Likewise, Fcγ receptors (FcγR) I (CD64), II (CD32), and III (CD16) were expressed on the cell surface. Among Fcγ receptors, CD32, which is the most important receptor for immune complex uptake, was most strongly expressed (Fig. 3*F*). Moreover, the activating isoform CD32A displayed considerably higher expression levels than CD32B/C molecules (Fig. 3*G*). The differentiated DD-ME macrophages displayed greater upregulation of MHC class I (A, B, C) and II (DR, DQ, DP) molecules, compared with the undifferentiated cells (Fig. 3*H*). Analysis of the transcription of selected monocytic genes revealed overlapping M1 and M2 characteristic targets, including IL-6 and IL-10 expression in differentiated and LPS-activated phagocytes (Fig. 3 *I* and *J*). Several reports have described MLL-r

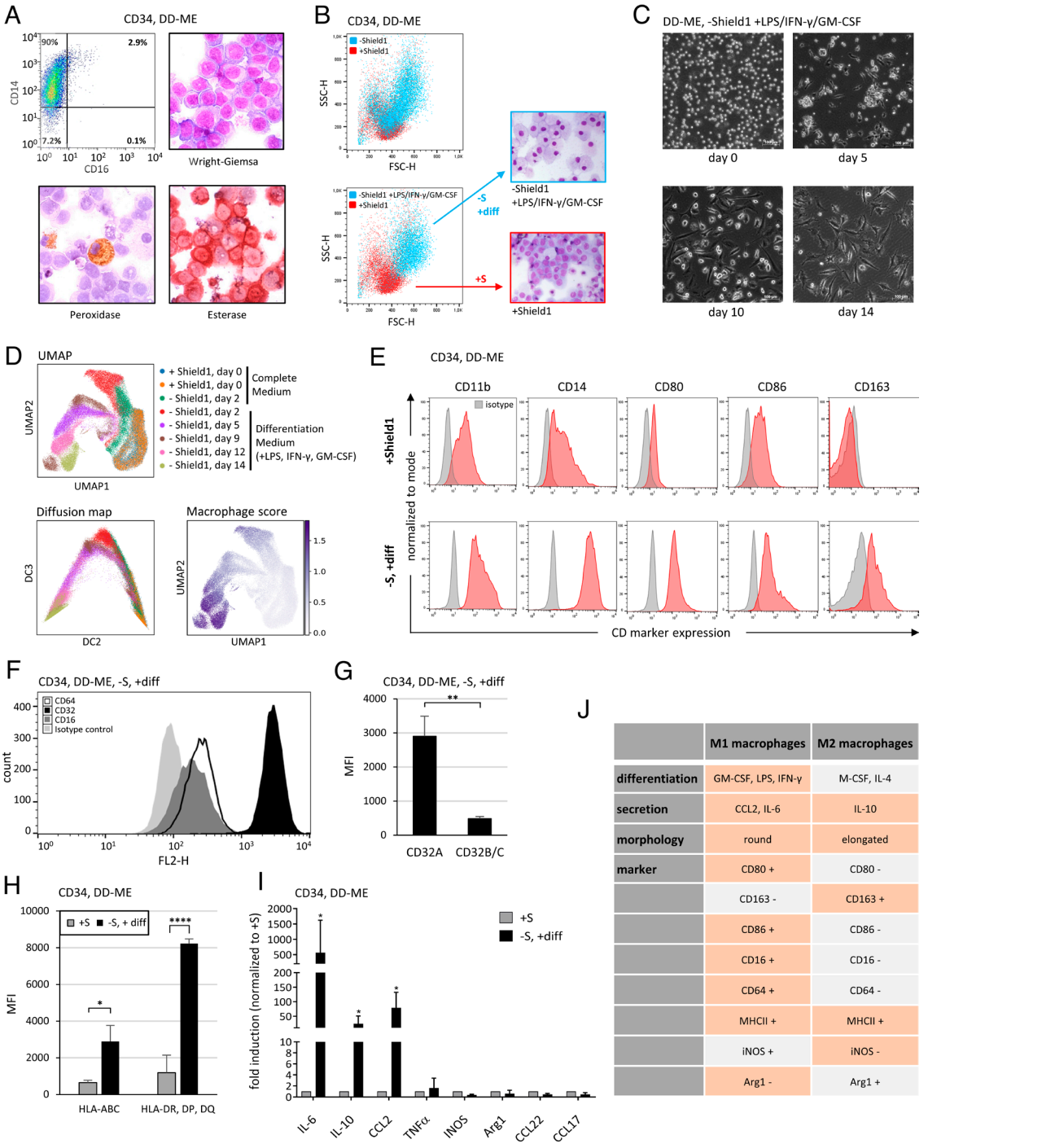

Fig. 3. Morphological characterization of DD-ME cells in the presence and absence of Shield1. (*A*) CD14, CD16, and hematology stainings of DD-ME expressing cells at day 43 posttransduction in the presence of Shield1 (Wright-Giemsa, peroxidase, and esterase). (*B*) DD-ME cells at day 43 posttransduction were deprived of Shield1 and cultured in either complete medium or medium containing LPS (100 ng/mL), IFN-γ (20 ng/mL), and GM-CSF (20 ng/mL) for 6 d. Morphology of the differentiated cells (blue) was analyzed via flow cytometry and cytospin preparations and compared with DD-ME cells +Shield1 (red). (*C*) Morphology shift of DD-ME cells during 14 d of differentiation in the presence of LPS, IFN-γ, and GM-CSF without Shield1. (*D*) DD-ME cells were harvested at different time points of monocytic differentiation to be used for single cell RNA (scRNA) sequencing. The cells' RNA profiles are visualized using Uniform Manifold Approximation and Projection (UMAP) reflecting the topology of cells in the high-dimensional graph. The diffusion map visualization (*Bottom Left*) displays the differentiation trajectories present in the cell graph. The diffusion components DC2 and DC3 are shown. Each color represents cells from one of the eight different samples. The right UMAP shows the macrophage gene set score obtained using marker genes from the automated cell type annotation tool Celltypist (Immune_all_High model). (*E*) Flow cytometry analysis of macrophage-associated cell surface marker expression on DD-ME +Shield1 cells compared with differentiated DD-ME cells at day 14. The depicted analysis is representative of three biological replicates. (*F*) Flow cytometry analysis of FcγR III (CD16), FcγR II (CD32), FcγR I (CD64) expression on differentiated DD-ME cells. The depicted histogram is representative of three biological replicates. (*G*) Assessment of mean fluorescence intensities (MFI) after surface staining of the activating CD32 A-isoform and the CD32 B/C-isoforms on differentiated DD-ME cells. The data are presented as the mean plus the SD of three biological replicates. Statistical significance was calculated with a two-tailed *t* test. (*H*) Assessment of MFI after staining of HLA-ABC and HLA-DR/DQ/DP prior and upon differentiation. The data are presented as the mean plus the SD of three biological replicates. Statistical significance was calculated with a two-tailed *t* test. (*I*) qRT-PCR analysis of pro- and anti-inflammatory genes prior and upon differentiation. Fold induction in reference to +Shield1 control group was calculated with actin as a reference gene. The data are presented as the mean plus the SD of three biological replicates. Statistical significance was calculated with a Mann–Whitney *U* test. (*J*) The key features of M1 and M2 macrophages. The peach colored cells indicate the properties of the differentiated DD-ME phagocytes. FSC, forward scatter; SSC, side scatter. For all statistical analyses, * indicates $P < 0.05$, ** indicates $P < 0.01$, *** indicates $P < 0.001$, and **** indicates $P < 0.0001$.

leukemic blasts with mixed myeloid/lymphoid phenotypes (40, 41); however, we did not detect the expression of lymphocytic markers such as CD3, CD8, CD19, and CD20. Furthermore, we did not detect the expression of granzyme B and perforin, two T cell effector proteins, while CEBPα and NF-kB were both expressed. Accordingly, we did not detect a response to T cell stimulation (*SI Appendix*, Fig. S12 *A–C*). Moreover, to evaluate differentiation into cell types other than macrophages, we changed the cytokine setting favoring differentiation into either megakaryocytes or erythrocytes. However, even in co-culture with OP9 stromal cells, differentiated DD-ME cells did not express characteristic markers of those cell types. Instead, the cells expressed CD14 and CD11b suggesting DD-ME cells as primed late monocytic progenitor cells (*SI Appendix*, Fig. S4*D*).

Enrichment of Genes Involved in Innate Immunity in Differentiated DD-ME Macrophages. To investigate the gene expression signatures of DD-ME macrophages, we analyzed mRNA using a myeloid cell innate immunity panel of 770 genes and a Nanostring nCounter System. We conducted a gene expression analysis of human CD34+ cells, Shield1-expanded progenitors (DD-ME+S), differentiated DD-ME phagocytes, and PBMC-derived CD14-isolated monocytes derived from healthy donors as naïve monocytic control cells in biological triplicates. Analysis of genes important for differentiation and maintenance of myeloid cells revealed marked similarity between differentiated DD-ME cells and isolated naïve CD14+ monocytes in contrast to CD34+ cells and DD-ME progenitors. Essential genes for DNA replication and cell cycle, including *MSH2*, *MCM5*, *TOP2A*, and *BIRC5*, were markedly down-regulated in DD-ME macrophages and CD14+ monocytes, which is a distinctive feature of terminally differentiated myeloid cells. In accordance, gene sets indicative of cell cycle arrest and differentiation, such as *MYOD1* and *MAFB*, were up-regulated (Fig. 4*A*). Furthermore, principal component analysis (PCA) revealed a clear separation in PC1 vs. PC2, thus indicating similarities between monocytes and differentiated DD-ME cells in PC1 and differences between all four cell types in PC2 (Fig. 4*B*). Additionally, analysis of genes involved in macrophage function in the DD-ME phagocytes yielded a high "macrophage score," as calculated by the average of the $\log_2$ expression (Fig. 4*C*). Likewise, when classifying single genes into innate immunity-specific subsets such as Fc receptor signaling, antigen presentation, and TH1/TH2 activation, both the differentiated DD-ME cells and the CD14+ monocytes showed similar expression patterns and markedly differed from the CD34+ cells and the DD-ME+S progenitor cells (Fig. 4*D*). Moreover, DD-ME macrophages displayed significant upregulation of genes involved in migration and adhesion, thus resembling the expression pattern of human peripheral blood-derived CD14+ monocytes (Fig. 4*E*). We also compared the expression levels of selected genes involved in proliferation, including *BIRC5, CCNB2, TOP2A, CDC20, MYC*, and *TTK*, and detected a complete downregulation upon Shield1 removal and differentiation (Fig. 4*F*). Assessment of genes involved in immune pathways revealed marked upregulation of key mediators in chemokine signaling, toll-like receptor signaling, and TNF signaling—crucial for the recruitment of various immune cells—upon differentiation of the DD-ME cells (*SI Appendix*, Fig. S13 *A–C*).

DD-ME Macrophages Adhere to VCAM-1 under Shear Stress and Migrate toward the Chemokine CCL2. We next aimed to determine whether the DD-ME phagocytes featured typical adhesion and migration properties of primary macrophages. We found that differentiated DD-ME cells adhered to tissue culture-treated surfaces (Fig. 3*C*). Upon culture in Monocyte Attachment Medium, the majority of the differentiated DD-ME macrophages attached to plastic surfaces compared with the undifferentiated DD-ME cells and T cells, which served as controls (Fig. 5*A*). To analyze the macrophage adhesion properties under shear stress, we mimicked the in vivo blood vessel environment using a flow chamber assay. Accordingly, the DD-ME macrophages were incubated on either uncoated µ-slides or ligand substrate VCAM-1-coated µ-slides for 5 min before the flow speeds were increased. Even at major shear stress, approximately one third of the macrophages remained attached to the slides via VLA-4 binding to VCAM-1, whereas all macrophages on uncoated slides detached at low speeds (Fig. 5*B*).

Macrophages migrate toward infected or injured areas during injury and subsequent inflammation. To analyze the migration properties of the DD-ME-derived macrophages, we conducted a 3D chemotaxis assay on µ-slides using the chemokine monocyte chemoattractant protein 1 (MCP-1/CCL2) as an inflammatory recruiting stimulus. Undifferentiated DD-ME cells were used as control. Both cell types were monitored for 2 h on slides with and without CCL2 gradient and subsequently analyzed for movement, by recording velocity and accumulated distance. When incubated in the presence of a CCL2 gradient, DD-ME macrophages and the undifferentiated DD-ME cells migrated toward CCL2, although the macrophages traveled a significantly farther accumulated distance and migrated at a greater velocity. In the absence of the chemoattractant, no specific directional movement was observed (Fig. 5 *C* and *D*).

Engineered Phagocytes Are Able to Engulf Bacterial Microparticles, Cell Debris, and Apoptotic Cells and Efficiently Phagocytize Lymphoma Cells in an Antibody-Dependent Manner. We then assessed whether DD-ME-derived macrophages could phagocytize bacterial particles. The differentiated macrophages were first coincubated with *Escherichia coli*-derived pHrodo™ BioParticle conjugates. After 15 min of coincubation, macrophages displayed a clear fluorescence signal detected by flow cytometry, which reflected the uptake of the conjugates into acidic phagosomes. Similar findings were obtained with primary CD14+ monocytes isolated from PBMCs, in which naive T cells were used as a negative control (Fig. 6*A*). BioParticle uptake was completely blocked by pretreatment with the phagocytosis inhibitor cytochalasin D (Fig. 6*B*). The phagocytes were also competent in reactive oxygen species production as shown by staining with CellROX deep red reagent (Fig. 6*C*). During the course of the experiments, we noticed a distinct decrease in both apoptotic and dead cells in the differentiated DD-ME cell culture, thereby suggesting that the engineered macrophages had indeed engulfed the cellular debris (Fig. 6*D*). Phagocytosis of dead and dying cells was also demonstrated using staurosporine pretreated Jurkat cells in an efferocytosis assay (Fig. 6*E*). As DD-ME-induced phagocytes express surface Fcγ receptors, we aimed to verify binding to human antibodies. We observed binding of IgG, by applying various concentrations of human immune globulin protein (Gamunex) (Fig. 6*F*).

To assess the removal of opsonized target cells, which is a pivotal function of macrophages, we used the Burkitt's lymphoma cell lines Daudi and Raji as well as patient-derived mantle cell lymphoma cells to perform antibody-dependent cellular phagocytosis (ADCP) assays at an effector-target ratio of 1:2 in the presence of the therapeutic antibodies rituximab and daratumumab. When incubated with Daudi cells, we observed phagocytosis rates above 50% in the presence of rituximab, which targets CD20 (i.e., half of the quantified macrophages engulfed at least one lymphoma target cell). Similarly, we observed phagocytosis rates of 40% in the presence of daratumumab, which targets CD38 (Fig. 6*G*). Using Raji cells as a target, we demonstrated phagocytosis rates of 30% with rituximab and 20% with daratumumab (Fig. 6*H*). Assessment of patient-derived leukemic mantle cell lymphoma cells revealed 20% phagocytosis with rituximab, while no effect was observed with daratumumab, as CD38 expression levels were very low (Fig. 6 *I* and *J*). In each

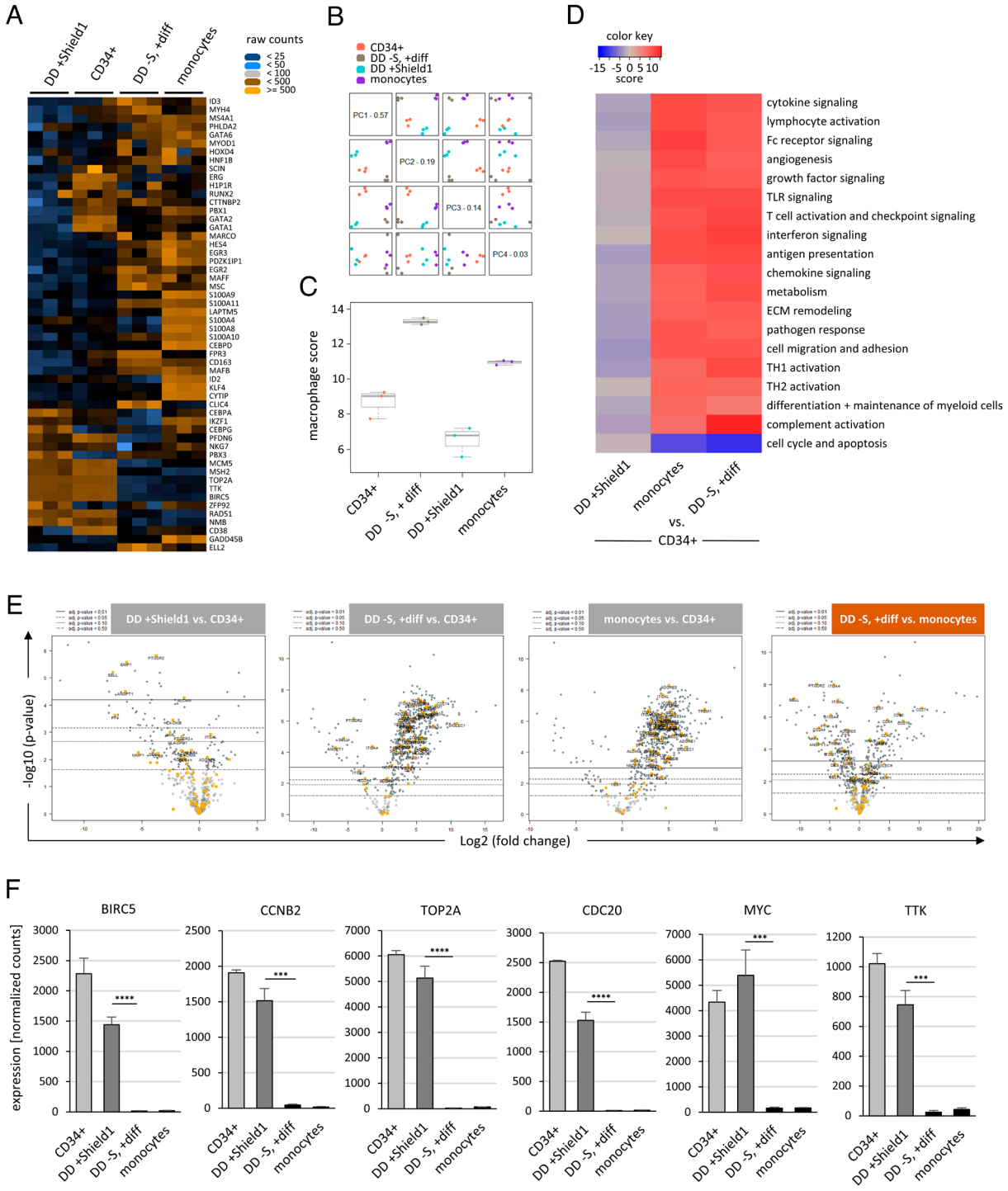

Fig. 4. Myeloid target gene expression in nontransduced CD34+ cells, DD-ME+S cells, differentiated DD-ME cells, and PBMC-derived naïve CD14+ monocytes. (*A*) Heat map evaluation of 52 target genes involved in myeloid cell differentiation and maintenance in nontransduced CD34+ cells, DD-ME+S cells (DD +Shield1), DD-ME macrophages (DD −S, +diff), and PBMC-derived CD14+ monocytes (monocytes). The depicted gene set is part of the 770 gene myeloid innate immunity panel which was analyzed via Nanostring nCounter Systems. The results of three biological replicates are represented. (*B*) Principal component analysis (PCA) plot of the gene expression data displaying all genes involved in myeloid cell differentiation and maintenance. The four principal components capture the highest level of variance. (*C*) Cell type profiles of the gene expression samples using the Nanostring advanced analysis module with the macrophage score for each sample. The average log2 of the expression levels of the macrophage marker genes are shown. (*D*) Heat map of directed global significance score illustrating clustered genes grouped according to immune cell function. Three replicates were pooled for each group, which were compared with baseline expression levels in CD34+ cells. Up-regulated gene groups are shown in red, while down-regulated gene groups are shown in blue. (*E*) Differential expression analysis of genes involved in cell migration and cell adhesion. For each gene (yellow dot) analyzed in the DD-ME+S, DD-ME macrophage (−S, +diff), and monocyte samples, a linear model was fit assessing the log2 transformed and normalized expression levels in CD34+ cells. The volcano plot illustrates the log10 (*P*-value) and log2 fold change for each gene as compared with CD34+ cells or monocytes. Highly statistically significant genes are located at the top of the plot, while highly differentially expressed genes located along the x-axis. (*F*) Normalized gene expression levels of six core genes involved in proliferation in CD34+ cells, DD +Shield1, DD −S, +diff, and CD14+ monocytes. The data are presented as the mean plus the SD of three biological replicates. The expression results were obtained and normalized using the geometric means of six positive control genes and 40 housekeeping genes. Statistical significance was calculated with a one-way ANOVA with multiple comparisons. For all statistical analyses, *** indicates $P < 0.001$ and **** indicates $P < 0.0001$.

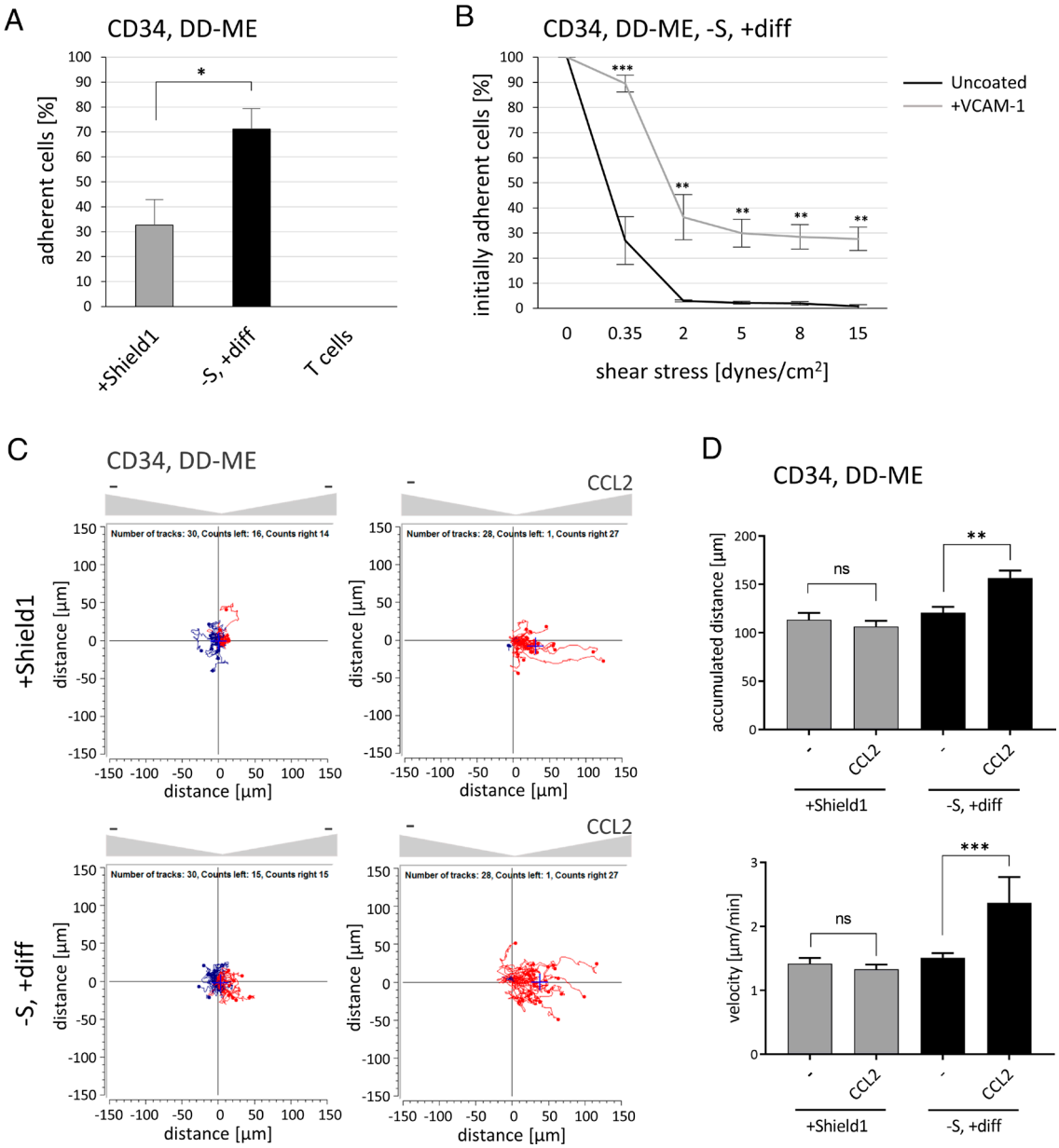

Fig. 5. Adhesion and migration properties of differentiated DD-ME cells. (*A*) After 6 d of differentiation, the adhesion capacity of DD-ME cells was analyzed in Monocyte Attachment Medium on a tissue culture-treated 24-well plate, compared with DD-ME cells +Shield1 and freshly isolated T cells. The data are presented as the mean plus the SD of three technical replicates. Statistical significance was calculated with a one-way ANOVA. (*B*) The differentiated DD-ME cells were incubated for 5 min on either uncoated or VCAM1-coated ibidi µ-slides before applying continuous and increasing flow speeds of buffer using an automated syringe. The adherent cells were quantified via microscopy at each step before the flow speed was increased. The data are presented as the mean plus the SD of three biological replicates. Statistical significance was calculated with unpaired *t* tests. (*C*) 3D-chemotaxis assay of DD-ME+S cells and differentiated DD-ME cells embedded in a gel matrix and subjected to control medium (−) or CCL2 (300 ng/mL) chemoattractant gradients using Ibidi µ-slides. Cell migration was traced for 2 h using live cell microscopy and analyzed via manual tracking. Each migration route represents the movement of a single cell, in which migration toward CCL2 is indicated in red. The blue crosshair indicates the center of mass after 2 h of migration. (*D*) Quantification of accumulated distance and migration velocity of DD-ME cells +Shield1 and differentiated DD-ME cells from the data obtained in Fig. 5*D*. The data are presented as the mean plus the SEM. For all statistical analyses, * indicates $P < 0.05$, ** indicates $P < 0.01$, and *** indicates $P < 0.001$.

experiment, the HER2-specific antibody trastuzumab was used as a negative control, which exhibited the same level of background phagocytosis as the "without antibody" control. The phagocytic effect was further enhanced by targeting CD47, a potent "don't eat me" signal, using an Fc silent IgG2σ variant of the antibody magrolimab (hu5F9-G4) with abrogated C1q and FcγR binding. This observation was demonstrated when rituximab was combined with CD47 blockade, which yielded phagocytosis rates close to 70% when Daudi cells were used as targets (Fig. 6*K*). Additionally, CD47 blockade in combination with rituximab resulted in efficient engulfment of primary chronic lymphocytic leukemia cells isolated from patient-derived peripheral blood (*SI Appendix*, Fig. S14). Assessment of M0 and M1 macrophages from isolated PBMCs and nontransduced CD34+ in vitro-derived macrophages revealed a level of phagocytosis capacity similar to that of the DD-ME-derived phagocytes (Fig. 6*L*). Furthermore, fluorescence microscopy revealed the phagocytic uptake of CFSE-labeled Daudi cells (Fig. 6*M*). Overall, we demonstrate the exploitation of the chimeric fusion protein ME for large-scale expansion of human hematopoietic monocytic progenitor cells and subsequent differentiation into functional macrophage-like cells able to engulf opsonized target lymphoma cells (Fig. 6*N*).

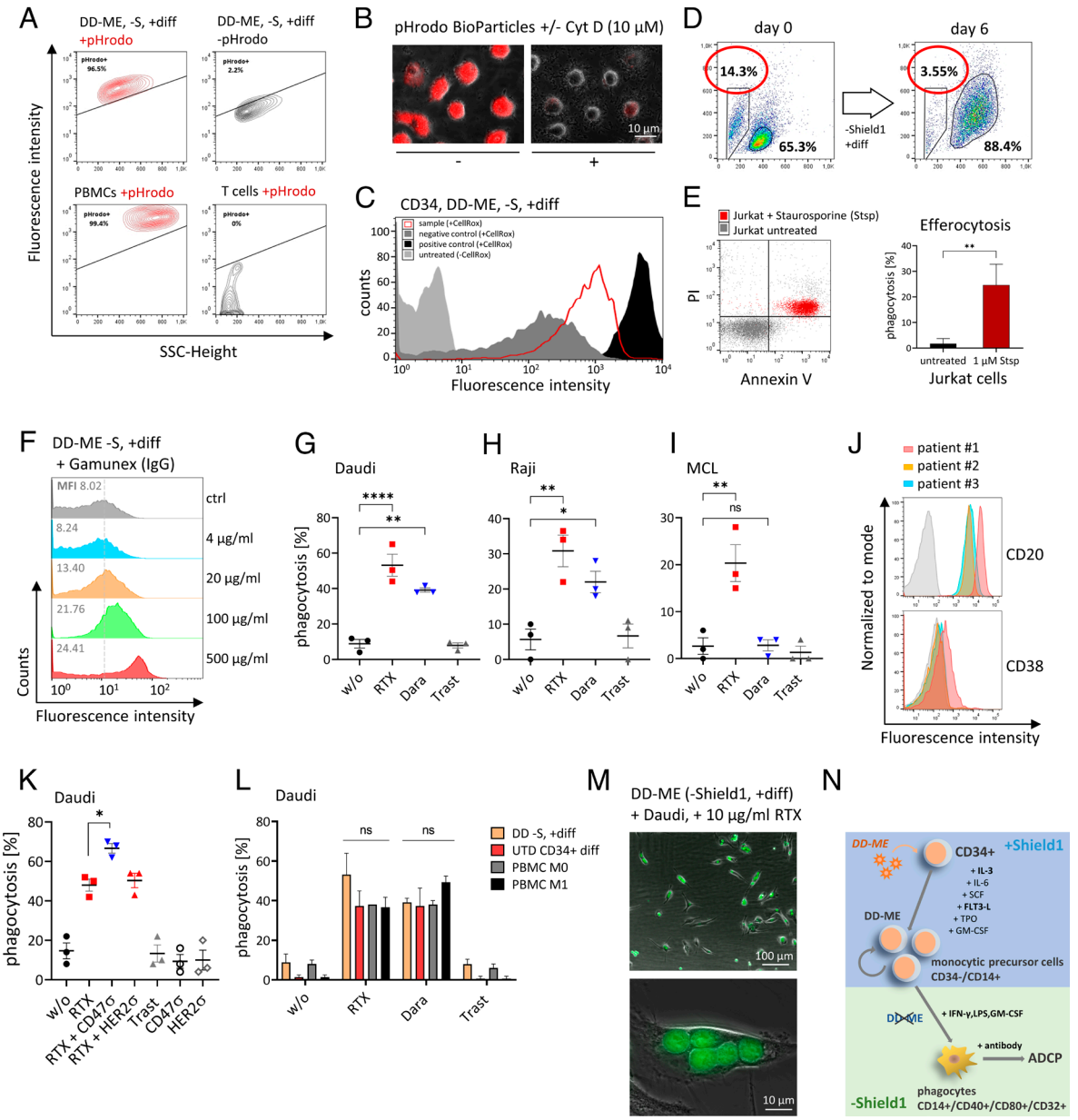

Fig. 6. Functional characterization of differentiated DD-ME cells. (*A*) Phagocytosis assay with differentiated DD-ME cells, PBMC-derived CD14+ monocytes, and T cells incubated with pHrodo Red *E. coli* BioParticles (effector-target ratio 1:20). Upon pHrodo BioParticle uptake, an enhanced fluorescence signal was observed upon acidification in the phagosome. (*B*) To verify the uptake of pHrodo BioParticles via phagocytosis, differentiated DD-ME cells were pretreated with 10 µM Cytochalasin D (Cyt D). (*C*) Detection of reactive oxygen species (ROS) in differentiated DD-ME cells via flow cytometry using CellROX deep red reagents. N-acetylcysteine was used as the negative control, while tert-butyl hydroperoxidase was used as the positive control. (*D*) DD-ME cells were analyzed for clearance of cell debris prior to differentiation and after 6 d of differentiation via flow cytometry. Forward and side scatter plots depicting undifferentiated, differentiated, and dead cells. (*E*) To assess cell efferocytosis capacity, differentiated DD-ME cells were coincubated with either live or apoptotic Jurkat cells at an effector-target ratio of 1:2. To induce cell death in Jurkat cells, 1 µM staurosporine was added to the medium for 4 h. (*F*) Assessment of antibody Fc fragment binding to DD-ME phagocytes using various concentrations of human immunoglobulin and secondary PE-conjugated anti-human IgG. (*G–I*) DD-ME cells were differentiated in medium containing LPS, IFN-γ, and GM-CSF (−Shield1) and coincubated with either CFSE-labeled Daudi, Raji, or patient-derived MCL cells with an effector-target ratio of 1:2 for 3 h in the presence of therapeutic antibodies (10 µg/mL). ADCP was assessed by quantifying phagocytized differentiated cells via fluorescence microscopy. The data are presented as the mean plus the SD of three biological replicates. Statistical significance was calculated with one-way ANOVA and multiple comparisons. (*J*) CD20 and CD38 expression levels of the patient-derived MCL cells used for the ADCP assay. (*K*) Increased phagocytosis was observed by further inhibiting the "don't eat me" signal, CD47 expressed on target cells, using an engineered Fc silent CD47-IgG2 antibody (10 µg/mL) referred to as CD47σ. An IgG2 version of trastuzumab (HER2σ) was used as a control. Statistical significance was calculated with one-way ANOVA and multiple comparisons and data represent the mean ± SD of three biological replicates. (*L*) Phagocytosis capacity was assessed with M0 and M1 macrophages generated from isolated PBMCs and nontransduced CD34+ cell-derived macrophages as compared with macrophages generated from differentiated DD-ME cells. Data are represented as the mean plus the SD of three biological replicates. (*M*) Fluorescence microscopy of engulfed Daudi cells after coincubation with differentiated DD-ME cells. (*N*) Graphical abstract of the macrophage production procedure. Cyt D, cytochalasin D; RTX, rituximab; Dara, daratumumab; Trast, trastuzumab; and MCL, mantle cell lymphoma. For all statistical analyses, * indicates $P < 0.05$, ** indicates $P < 0.01$, *** indicates $P < 0.001$, and **** indicates $P < 0.0001$.

Discussion

In this study, we demonstrate that an adjustable leukemia-associated fusion protein can be used to control the expansion of HSPCs and subsequent differentiation into fully functional blood cells. We utilized an MLL-ENL chimeric fusion gene that is frequently found in AML with monocytic maturation (27, 32) fused to an adjustable protein stabilization domain. Exploiting this modified form of MLL-ENL with inducible progenitor expansion capacity, we describe demonstration of a leukemia-associated fusion protein that can be used to produce functional human phagocytes in large scale suitable for experimental cell-based approaches.

Among the up-regulated transcripts, we observed high levels of MYC expression in DD-ME progenitors, which were completely down-regulated upon ME shutdown and monocytic differentiation. Accordingly, continuous MYC expression has been shown to block terminal myeloid differentiation at an intermediate stage during the progression from immature blast cells to mature macrophages (42). Similarly, we observed robust HOXA9 expression, which clearly disappeared once Shield1 was removed. Interestingly, we found that overexpression of several *HOX* genes alone, including *HOXB4*, *HOXB8*, and the direct ME target *HOXA9*, completely failed to induce human CD34+ liquid cell culture expansion, contrary to observations in murine progenitor cells (43–45). Despite a loss of CD34 surface marker expression, DD-ME-expanded progenitors presented a similar gene expression pattern compared with unmodified naïve CD34+ cells. This observation indicates that the DD-ME expanded cells exhibit progenitor-like characteristics. Under the culture conditions used, which are known to promote a myelomonocytic cell fate, continuous MLL fusion protein activity mediated the sustained proliferation of an immature monocytic phenotype. In the presence of Shield1 plus IL-3 and Flt3-L, these monocytic precursors continued to self-renew without further differentiation. Notably, the receptor of Flt3-L, Flt3 (FLK2), is not only expressed in hematopoietic stem cells to maintain stem cell survival, but also in granulocyte/macrophage progenitors (46, 47). In our liquid culture system, Shield1 removal functioned as a "break release" signal and, together with proinflammatory stimuli, resulted in terminal differentiation into fully functional macrophages. Global gene expression analysis revealed similar profiles for the DD-ME-derived phagocytes compared with naïve CD14-selected monocytes from the peripheral blood of healthy individuals. Furthermore, genes involved in innate immunity, such as FcγR signaling, lymphocyte activation, and antigen presentation, were up-regulated upon differentiation into DD-ME phagocytes comparable to PBMC-derived unmodified monocytes, thereby indicating that macrophages play a central role in immune cell coordination (48). The expansion and differentiation protocol even worked with a very low initial transduction rate of human CD34+ cells and steadily resulted in pure macrophages at an arbitrary time point of ex vivo expansion. Complete differentiation was only observed with cells deprived of Shield1, thus demonstrating that degradation of the adjustable fusion protein ME was required for terminal monocytic maturation steps. It could be speculated that the cellular debris remaining in the culture of proliferating and differentiating macrophages acts as an additional stimulus for maturation into M1/M2 inflammatory macrophages, which are able to engulf cell debris and apoptotic cells (49).

The method described presents several advantages over the classical collection procedures of blood cells from healthy donors (50). The engineered progenitors can be cryopreserved in a cell bank. The aspect of unlimited expansion enables large-scale production of highly homogenous cell progenitors. Although the iPSC-based technology is a promising method to produce differentiated cells in vitro, the method described here presents some advantages for the production of human blood cells. Reprogramming cells into iPSCs is laborious and time-consuming, including steps that are difficult to standardize such as isolation and extensive characterization of clones and the corresponding differentiation propensities. IPSCs are commonly grown as adherent cells, and transition into bioreactors represents a challenging task. Currently, directed differentiation of iPSCs into hematopoietic cells remains inefficient, which yields relatively low numbers of stem and progenitor cells that would require large-scale expansion (51, 52). Our strategy significantly reduces the number of steps and time necessary to generate sufficient numbers of progenitor and effector cells. In our approach, ME-programmed cells quickly outcompeted unmanipulated cells in culture, thus avoiding the need for clone enrichment or selection. As the programmed cells remain hematopoietic progenitors, they can be easily grown in liquid culture, thereby enabling rapid upscaling.

The monocytic precursors pass through an extensive ex vivo culture phase. During the expansion phase, proliferation is driven solely by MLL-ENL and, after induced degradation of the fusion protein following Shield1 removal, did not result in the formation of escape mutants, even after over a year of in vitro cultivation. Simultaneously, the cells are differentiated with stimuli, which do not permit progenitor self-renewal and expansion, allowing complete terminal differentiation. Several highly induced proliferation-associated genes detected in ME-DD+S progenitor cells were down-regulated in differentiated DD-ME cells to a level comparable to that of naïve monocytes, thus reflecting the low to absent proliferative capacity. Overall, reactivation of the DD-ME fusion protein and restored proliferation of the generated macrophages is extremely unlikely. We did not detect any escape mutants, even in cultures containing 10^9 undifferentiated cells, which were deprived of Shield1 and proliferation cytokines. They also completely failed to give rise to colonies in semisolid medium after differentiation. To ensure proliferation blockage, the cells could be further inactivated using gamma-irradiation (53). Subsequent studies should assess whether certain domains of either MLL or ENL can be deleted to spare unwanted oncogenic functions while preserving the stem/progenitor cell expansion capacity. Indeed, reducing the likelihood of inadvertently introducing potentially oncogenic elements might permit in vivo applications. The replacement of the MLL fusion partner by a simple dimerization domain has been shown to be sufficient to maintain the self-renewal-promoting activity of MLL chimeric genes, at least in murine progenitor cells (54–56). Using transient, nonintegrating expression systems may further help to avoid the genotoxic or oncogenic effects of retroviral vectors. Although γ-retro- and lentiviral vectors feature advantages such as sustained transgene expression, large packaging capacity, and low immunogenicity, their relatively random integration profile poses a substantial drawback (57, 58). Particular strategies exist to circumvent this issue, including the use of nonintegrating viral vectors, the sleeping beauty transposon system, or genome-editing technologies such as CRISPR/Cas. Nonintegrating viral vectors such as adenoviruses and adeno-associated viruses only mediate transient expression, though. In comparison, nonintegrating lentiviruses might possess more prolonged transgene expression rates (59). Apart from virus-based gene transfer, sustained transgene expression can also be obtained by integration using either the sleeping beauty transposon system displaying a favorable integration profile or targeted integration via genome-editing technologies such as TALEN and CRISPR/Cas (60, 61). These strategies provide potential directions for further development of our approach. Finally, the biological activity of such produced phagocytes has to be analyzed in appropriate in vivo model systems.

The adjustable design of the human primary cell system described in this study is highly useful to study transcriptional programs of immature and differentiated blood immune cells. Such phagocytes

can be utilized in a wide variety of studies such as modeling infection biology approaches in human macrophages (62, 63) and wound healing studies in humanized animal models (64). The phagocytes produced in this study can also be equipped with a CAR coding sequence to generate target-specific, anticancer CAR phagocytes for experimental, preclinical cell therapy approaches (30).

Overall, we describe demonstration of a leukemia-associated gene product used to both expand human blood progenitor cells ex vivo and maintain the cell's ability to differentiate in a controlled manner, with specific immune cell functions preserved. These findings shed light into the oncogenic functions of MLL-ENL and strongly suggest that the phenotype of oncogene-transformed blood precursors is not necessarily irreversibly changed, even after more than 1 y of large-scale in vitro expansion calculated to $>10^{32}$-fold. This method may also be applied for other fusion genes and differentiation stimuli. Such adjustable fusion proteins have the potential to serve as effective molecular tools to expand and differentiate human blood progenitors into functional immune cells suitable for experimental cell-based approaches.

Materials and Methods

Retroviral Vector Construction and Transduction. The coding sequence of the destabilization domain FKBP12(F36V,E31G,R71G,K105E) (65) was synthesized (Geneart) and fused at the N terminus of MLL-ENL in an MSCV-based retroviral expression vector (kindly provided by Rolf Marschalek, University Frankfurt, Germany). The sequences of *HOXB8* (synthesized by Geneart) and *HOXA9* (Addgene #97041) were cloned into the same retroviral backbone. Retroviral transduction of human bone marrow–derived CD34+ cells (Lonza, Cologne, Germany) was performed as previously described (66).

Cell Culture. Culture conditions for cell lines and primary cells are described in *SI Appendix*.

Isolation of Human Primary Stromal Cells. Details regarding isolation of human primary stromal cells are provided in *SI Appendix*.

Spheroid Formation and DD-ME Cell Proliferation. Details regarding hMSC-derived spheroid formation and DD-ME cell proliferation upon coculture are provided in *SI Appendix*.

PBMC Isolation, Differentiation, and Colony-Forming Assay. The protocols pertaining to PBMC isolation, differentiation, and colony-forming unit assays are described in *SI Appendix*.

Flow Cytometry. All flow cytometry analyses were performed using a BD FACSCalibur. Flow cytometry data were analyzed using Cellquest Pro 6.0 and FlowJo v10.6.2 software. The antibodies used for staining are listed in *SI Appendix*.

Western Blot. The cell lysates were prepared and the immunoblots were performed as previously described (67). The antibodies used for western blot analysis are listed in *SI Appendix*.

Chromosome Analysis, Telomere Length Measurement, and Whole Exome Sequencing. Details regarding chromosome analysis, telomere length measurement, and whole exome sequencing are provided in *SI Appendix*.

Flow Chamber Adhesion Assay and Migration Assay. To analyze the adhesion behavior of the differentiated DD-ME cells under shear stress, we performed flow chamber adhesion assays as previously described (68) and provided in detail in *SI Appendix*. To analyze cell migration behavior, differentiated DD-ME cells and DD-ME +Shield1 cultivated cells were analyzed in a 3D migration assay using 3D chemotaxis µ-slides (ibidi) with an adapted protocol as previously described (69). Additional details are provided in *SI Appendix*.

Ligation-Mediated PCR (LM-PCR), TOPO Cloning, and Sequencing. Details regarding analysis of retroviral integration sites via LM-PCR and subsequent TOPO cloning and sequencing are provided in *SI Appendix*.

Single Cell RNA Sequencing. Details regarding single cell RNA sequencing are provided in *SI Appendix*.

RNA Expression Analysis via NanoString nCounter System. Details regarding sample preparation and RNA expression analysis are provided in *SI Appendix*.

qRT-PCR. Isolated RNA was transcribed into cDNA using the First Strand cDNA Synthesis Kit (Thermo Scientific) according to the manufacturer's protocol. qRT-PCR samples were prepared with cDNA, ORA™ SEE qPCR Green ROX L Mix, 2X (highQu), and specific primers for the genes of interest. qRT-PCR was performed using a Rotor-Gene Q thermocycler (Qiagen). The data were evaluated using the $2^{-\Delta\Delta Ct}$ method. The primer sequences are listed in *SI Appendix*.

Reactive Oxygen Species Detection and *E. coli* BioParticle Uptake Assay. Detailed information regarding the reactive oxygen species detection and *E. coli* BioParticle uptake assay are provided in *SI Appendix*.

Efferocytosis Assay and ADCP Assay. Detailed information regarding the efferocytosis and ADCP assays are provided in *SI Appendix*.

Statistical Analysis. Statistical differences were analyzed using GraphPad Prism 8.0 with the unpaired Student's *t* test or ANOVA for multiple comparison. For all statistical analyses, * indicates $P < 0.05$, ** indicates $P < 0.01$, *** indicates $P < 0.001$, **** indicates $P < 0.0001$, and ns indicates nonsignificant.

Data, Materials, and Software Availability. Single cell RNA-seq raw count matrices and raw fastq files are available on GEO (GSE237826) (70). Bulk Nanostring data and reproducibility notebooks and RNA-seq data are available on Zenodo (DOI: 10.5281/zenodo.8169407) (71) and Github (https://github.com/DaneseAnna/reproducibility_Windisch_2023_sc) (72).

ACKNOWLEDGMENTS. We thank Sandra Moore (Aix-Marseille University, France) for proofreading the manuscript and providing critical comments. We also thank Omar El Bounkari (LMU Munich, Germany) for help with the migration experiments and Michael Heide (LMU Munich, Germany) and the DKFZ Munich Core Facility for Digital Single Molecule Quantification (nCounter, NanoString). We are grateful to Inti Alberto De La Rosa Velázquez (Helmholtz Munich) for his technical expertise and help to enable single cell RNA sequencing in the Core Facility Genomics. Additional sequencing was conducted at the NGS and Data Technologies Core Unit of the Leibniz Institute for Immunotherapy (LIT, Regensburg). We are supported by the following research grants: Else Kröner-Fresenius-Stiftung No. 2021-EKSE.92 (P.A.G. and C.W.), Volkswagen-Stiftung No. 97103 (C.W.), Friedrich-Baur-Stiftung FB 25/16 & FB 20/17 (C.W.) and FB72/20 (A. Hoffmann), Metiphys program of the LMU Munich (A. Hoffmann), Deutsche José Carreras Leukämie Stiftung DJCLS 05 FN/2019 (S.V.), Wilhelm Sanders-Stiftung No. 2014.162.2 and 2014.162.3 (P.A.G. and C.W.). Deutsche Forschungsgemeinschaft (DFG) SFB1123-A3 (J. Bernhagen) DFG under Germany's Excellence Strategy within the framework of the Munich Cluster for Systems Neurology EXC 2145 SyNergy-ID 390857198 (J. Bernhagen) Munich Clinician Scientist Program (P.A.G.) German Research Foundation (DFG STR 1385/5-1) (A.D.).

Author affiliations: [a]Division of Transfusion Medicine, Cell Therapeutics and Haemostaseology, University Hospital, Ludwig-Maximilians-Universität München, Munich 81377, Germany; [b]Vascular Biology, Institute for Stroke and Dementia Research, Ludwig-Maximilians-Universität München, Munich 81377, Germany; [c]Department of Anesthesiology, University Hospital, Ludwig-Maximilians-Universität München, Munich 81377, Germany; [d]Biomedical Center, Department of Physiological Genomics, Ludwig-Maximilians-Universität München, Munich 81377, Germany; [e]Department of Medicine III, University Hospital, Ludwig-Maximilians-Universität München, Munich 81377, Germany; [f]German Cancer Consortium, Partner site Munich, Munich 81377, Germany; [g]German Cancer Research Center, Heidelberg 69120, Germany; [h]Division of Oncology, Department of Internal Medicine, Medical University of Graz, Graz 8010, Austria; [i]Georg-Speyer-Haus, Institute for Tumor Biology and Experimental Therapy, Frankfurt am Main 60596, Germany; [j]Department of Internal Medicine III, University Hospital Regensburg, Regensburg 93053, Germany; [k]Leibniz Institute for Immunotherapy, Regensburg 93053, Germany; [l]Laboratory for Leukemia Diagnostics, Department of Medicine III, University Hospital, Ludwig-Maximilians-Universität München, Munich 81377, Germany; [m]Institute of Human Genetics, University Hospital, Ludwig-Maximilians-Universität München, Munich 81377, Germany; [n]Department of Hematology, Oncology, Hemostaseology and Stem Cell Transplantation, Medical Faculty University Hospital Aachen, Rheinisch-Westfälische Technische Hochschule Aachen, Aachen 52074, Germany; [o]Division of Antibody-Based Immunotherapy, Department of Medicine II, Christian Albrechts University of Kiel, Kiel 24105, Germany; [p]Pediatric Hematology and Oncology, Department of Pediatrics III, University Hospital Essen and the University of Duisburg-Essen, Essen 45147, Germany; [q]Munich Cluster for Systems Neurology, Munich 81377, Germany; [r]Institute for Transfusion Medicine, University Hospital Essen, Essen 45147, Germany; [s]Institute for Transfusion Medicine and Cell Therapeutics, University Hospital Aachen, Rheinisch-Westfälische Technische Hochschule Aachen, Aachen 52074, Germany; [t]Division of Pediatric Hematology/Oncology, Boston Children's Hospital, Dana-Farber Cancer Institute, Harvard Medical School, Boston, MA 02115; and [u]Institute of General Pharmacology and Toxicology, University Hospital Frankfurt, Goethe-University, Frankfurt am Main 60596, Germany

1. A. Wilson, A. Trumpp, Bone-marrow haematopoietic-stem-cell niches. *Nat. Rev. Immunol.* **6**, 93–106 (2006).
2. S. J. Morrison, D. T. Scadden, The bone marrow niche for haematopoietic stem cells. *Nature* **505**, 327–334 (2014).
3. G. M. Crane, E. Jeffery, S. J. Morrison, Adult haematopoietic stem cell niches. *Nat. Rev. Immunol.* **17**, 573–590 (2017).
4. K. Takahashi, S. Yamanaka, Induction of pluripotent stem cells from mouse embryonic and adult fibroblast cultures by defined factors. *Cell* **126**, 663–676 (2006).
5. C. Lavau, S. J. Szilvassy, R. Slany, M. L. Cleary, Immortalization and leukemic transformation of a myelomonocytic precursor by retrovirally transduced HRX-ENL. *EMBO J.* **16**, 4226–4237 (1997).
6. J. C. Mulloy *et al.*, The AML1-ETO fusion protein promotes the expansion of human hematopoietic stem cells. *Blood* **99**, 15–23 (2002).
7. J. C. Mulloy *et al.*, Maintaining the self-renewal and differentiation potential of human CD34+ hematopoietic cells using a single genetic element. *Blood* **102**, 4369–4376 (2003).
8. F. Barabe, J. A. Kennedy, K. J. Hope, J. E. Dick, Modeling the initiation and progression of human acute leukemia in mice. *Science* **316**, 600–604 (2007).
9. A. M. Abdul-Nabi, E. R. Yassin, N. Varghese, H. Deshmukh, N. R. Yaseen, In vitro transformation of primary human CD34+ cells by AML fusion oncogenes: Early gene expression profiling reveals possible drug target in AML *PLoS One* **5**, e12464 (2010).
10. F. Faridi *et al.*, Aberrant epigenetic regulators control expansion of human CD34+ hematopoietic stem/progenitor cells. *Front Genet.* **4**, 254 (2013).
11. I. Sloma *et al.*, Ex vivo expansion of normal and chronic myeloid leukemic stem cells without functional alteration using a NUP98HOXA10homeodomain fusion gene. *Leukemia* **27**, 159–169 (2013).
12. K. Y. Chung *et al.*, Enforced expression of NUP98-HOXA9 in human CD34(+) cells enhances stem cell proliferation. *Cancer Res.* **66**, 11781–11791 (2006).
13. I. Sloma *et al.*, Epigenetic and functional changes imposed by NUP98-HOXA9 in a genetically engineered model of chronic myeloid leukemia progression. *Haematologica* **106**, 881–885 (2021).
14. C. Abramovich, N. Pineault, H. Ohta, R. K. Humphries, Hox genes: From leukemia to hematopoietic stem cell expansion. *Ann. N Y Acad. Sci.* **1044**, 109–116 (2005).
15. I. Fares *et al.*, Cord blood expansion. Pyrimidoindole derivatives are agonists of human hematopoietic stem cell self-renewal. *Science* **345**, 1509–1512 (2014).
16. A. E. Boitano *et al.*, Aryl hydrocarbon receptor antagonists promote the expansion of human hematopoietic stem cells. *Science* **329**, 1345–1348 (2010).
17. J. Chagraoui *et al.*, UM171 preserves epigenetic marks that are reduced in ex vivo culture of human HSCs via potentiation of the CLR3-KBTBD4 complex. *Cell Stem Cell* **28**, 48–62.e46 (2021).
18. S. Cohen *et al.*, Hematopoietic stem cell transplantation using single UM171-expanded cord blood: A single-arm, phase 1–2 safety and feasibility study. *Lancet Haematol.* **7**, e134–e145 (2020).
19. J. Singh *et al.*, Generation and function of progenitor T cells from StemRegenin-1-expanded CD34+ human hematopoietic progenitor cells. *Blood Adv.* **3**, 2934–2948 (2019).
20. A. C. Wilkinson *et al.*, Long-term ex vivo haematopoietic-stem-cell expansion allows nonconditioned transplantation. *Nature* **571**, 117–121 (2019).
21. D. C. Tkachuk, S. Kohler, M. L. Cleary, Involvement of a homolog of Drosophila trithorax by 11q23 chromosomal translocations in acute leukemias. *Cell* **71**, 691–700 (1992).
22. C. Meyer *et al.*, The MLL recombinome of acute leukemias in 2017. *Leukemia* **32**, 273–284 (2018).
23. J. Zhou, Y. Ng, W. J. Chng, ENL: Structure, function, and roles in hematopoiesis and acute myeloid leukemia. *Cell Mol. Life Sci.* **75**, 3931–3941 (2018).
24. D. T. Zeisig *et al.*, The eleven-nineteen–leukemia protein ENL connects nuclear MLL fusion partners with chromatin. *Oncogene* **24**, 5525–5532 (2005).
25. M. S. Cosgrove, A. Patel, Mixed lineage leukemia: A structure-function perspective of the MLL1 protein. *FEBS J.* **277**, 1832–1842 (2010).
26. B. E. Li, P. Ernst, Two decades of leukemia oncoprotein epistasis: The MLL1 paradigm for epigenetic deregulation in leukemia. *Exp. Hematol.* **42**, 995–1012 (2014).
27. T. Haferlach *et al.*, Distinct genetic patterns can be identified in acute monoblastic and acute monocytic leukaemia (FAB AML M5a and M5b): A study of 124 patients. *Br J. Haematol.* **118**, 426–431 (2002).
28. S. Schreiner *et al.*, MLL-ENL causes a reversible and myc-dependent block of myelomonocytic cell differentiation. *Cancer Res.* **61**, 6480–6486 (2001).
29. B. B. Zeisig *et al.*, Hoxa9 and Meis1 are key targets for MLL-ENL-mediated cellular immortalization. *Mol. Cell Biol.* **24**, 617–628 (2004).
30. M. Klichinsky *et al.*, Human chimeric antigen receptor macrophages for cancer immunotherapy. *Nat. Biotechnol.* **38**, 947–953 (2020).
31. L. A. Banaszynski, L. C. Chen, L. A. Maynard-Smith, A. G. Ooi, T. J. Wandless, A rapid, reversible, and tunable method to regulate protein function in living cells using synthetic small molecules. *Cell* **126**, 995–1004 (2006).
32. J. Reimer *et al.*, CRISPR-Cas9-induced t(11;19)/MLL-ENL translocations initiate leukemia in human hematopoietic progenitor cells in vivo. *Haematologica* **102**, 1558–1566 (2017).
33. M. Ashburner *et al.*, Gene ontology: Tool for the unification of biology. The gene ontology consortium. *Nat. Genet.* **25**, 25–29 (2000).
34. C. Gene Ontology, The gene ontology resource: Enriching a gold mine. *Nucleic Acids Res.* **49**, D325–D334 (2021).
35. H. Mi, A. Muruganujan, D. Ebert, X. Huang, P. D. Thomas, PANTHER version 14: More genomes, a new PANTHER GO-slim and improvements in enrichment analysis tools. *Nucleic Acids Res.* **47**, D419–D426 (2019).
36. M. P. Garcia-Cuellar, C. Buttner, C. Bartenhagen, M. Dugas, R. K. Slany, Leukemogenic MLL-ENL fusions induce alternative chromatin states to drive a functionally dichotomous group of target genes. *Cell Rep.* **15**, 310–322 (2016).
37. F. Beier *et al.*, Telomere length analysis in monocytes and lymphocytes from patients with systemic lupus erythematosus using multi-color flow-FISH. *Lupus* **16**, 955–962 (2007).
38. T. Hochstrasser, J. Marksteiner, C. Humpel, Telomere length is age-dependent and reduced in monocytes of Alzheimer patients. *Exp. Gerontol.* **47**, 160–163 (2012).
39. J. Wei *et al.*, Microenvironment determines lineage fate in a human model of MLL-AF9 leukemia. *Cancer Cell* **13**, 483–495 (2008).
40. O. K. Weinberg, D. A. Arber, Mixed-phenotype acute leukemia: Historical overview and a new definition. *Leukemia* **24**, 1844–1851 (2010).
41. O. Wolach, R. M. Stone, How I treat mixed-phenotype acute leukemia. *Blood* **125**, 2477–2485 (2015).
42. D. A. Liebermann, B. Hoffman, Differentiation primary response genes and proto-oncogenes as positive and negative regulators of terminal hematopoietic cell differentiation. *Stem Cells* **12**, 352–369 (1994).
43. J. Antonchuk, G. Sauvageau, R. K. Humphries, HOXB4-induced expansion of adult hematopoietic stem cells ex vivo. *Cell* **109**, 39–45 (2002).
44. G. G. Wang *et al.*, Quantitative production of macrophages or neutrophils ex vivo using conditional Hoxb8. *Nat. Methods* **3**, 287–293 (2006).
45. K. Izawa *et al.*, Activated HoxB4-induced hematopoietic stem cells from murine pluripotent stem cells via long-term programming. *Exp. Hematol.* **89**, 68–79.e67 (2020).
46. Y. Kikushige *et al.*, Human Flt3 is expressed at the hematopoietic stem cell and the granulocyte/macrophage progenitor stages to maintain cell survival. *J. Immunol.* **180**, 7358–7367 (2008).
47. S. W. Kim *et al.*, Flt3 ligand induces monocyte proliferation and enhances the function of monocyte-derived dendritic cells in vitro. *J. Cell Physiol.* **230**, 1740–1749 (2015).
48. L. Franken, M. Schiwon, C. Kurts, Macrophages: Sentinels and regulators of the immune system. *Cell Microbiol.* **18**, 475–487 (2016).
49. D. M. Mosser, J. P. Edwards, Exploring the full spectrum of macrophage activation. *Nat. Rev. Immunol.* **8**, 958–969 (2008).
50. E. S. Allen, C. Conry-Cantilena, Mobilization and collection of cells in the hematologic compartment for cellular therapies: Stem cell collection with G-CSF/plerixafor, collecting lymphocytes/monocytes. *Semin. Hematol.* **56**, 248–256 (2019).
51. A. Haase *et al.*, GMP-compatible manufacturing of three iPS cell lines from human peripheral blood. *Stem Cell Res.* **35**, 101394 (2019).
52. L. Lange *et al.*, Inducible forward programming of human pluripotent stem cells to hemato-endothelial progenitor cells with hematopoietic progenitor potential. *Stem Cell Rep.* **15**, 274 (2020).
53. M. M. Pelszynski, G. Moroff, N. L. Luban, B. J. Taylor, R. R. Quinones, Effect of gamma irradiation of red blood cell units on T-cell inactivation as assessed by limiting dilution analysis: Implications for preventing transfusion-associated graft-versus-host disease. *Blood* **83**, 1683–1689 (1994).
54. M. E. Martin *et al.*, Dimerization of MLL fusion proteins immortalizes hematopoietic cells. *Cancer Cell* **4**, 197–207 (2003).
55. C. W. So, M. Lin, P. M. Ayton, E. H. Chen, M. L. Cleary, Dimerization contributes to oncogenic activation of MLL chimeras in acute leukemias. *Cancer Cell* **4**, 99–110 (2003).
56. M. Eguchi, M. Eguchi-Ishimae, M. Greaves, The small oligomerization domain of gephyrin converts MLL to an oncogene. *Blood* **103**, 3876–3882 (2004).
57. K. E. Yoder, A. J. Rabe, R. Fishel, R. C. Larue, Strategies for targeting retroviral integration for safer gene therapy: Advances and challenges. *Front Mol. Biosci.* **8**, 662331 (2021).
58. L. Naldini *et al.*, In vivo gene delivery and stable transduction of nondividing cells by a lentiviral vector. *Science* **272**, 263–267 (1996).
59. A. Luis, The old and the new: Prospects for non-integrating lentiviral vector technology. *Viruses* **12**, 1103 (2020).
60. P. Kebriaei, Z. Izsvak, S. A. Narayanavari, H. Singh, Z. Ivics, Gene therapy with the sleeping beauty transposon system. *Trends Genet.* **33**, 852–870 (2017).
61. J. J. Kelly *et al.*, Safe harbor-targeted CRISPR-Cas9 homology-independent targeted integration for multimodality reporter gene-based cell tracking. *Sci. Adv.* **7**, eabc3791 (2021).
62. Z. Abassi, Y. Knaney, T. Karram, S. N. Heyman, The lung macrophage in SARS-CoV-2 infection: A friend or a foe? *Front. Immunol.* **11**, 1312 (2020).
63. M. Merad, J. C. Martin, Pathological inflammation in patients with COVID-19: A key role for monocytes and macrophages. *Nat. Rev. Immunol.* **20**, 355–362 (2020).
64. S. Y. Kim, M. G. Nair, Macrophages in wound healing: Activation and plasticity. *Immunol. Cell Biol.* **97**, 258–267 (2019).
65. E. L. Hagan, L. A. Banaszynski, L. C. Chen, L. A. Maynard-Smith, T. J. Wandless, Regulating protein stability in mammalian cells using small molecules. *Cold Spring Harb. Protoc.* **2009**, pdb prot5172 (2009).
66. C. Wichmann *et al.*, Activating c-KIT mutations confer oncogenic cooperativity and rescue RUNX1/ETO-induced DNA damage and apoptosis in human primary CD34+ hematopoietic progenitors. *Leukemia* **29**, 279–289 (2015).
67. C. Wichmann *et al.*, Dimer-tetramer transition controls RUNX1/ETO leukemogenic activity. *Blood* **116**, 603–613 (2010).
68. K. Ponnusamy *et al.*, The truncated RUNX1/ETO activates VLA-4-dependent adhesion and migration of hematopoietic progenitor cells. *Haematologica* **99**, e253–e256 (2014).
69. A. Hoffmann, L. C. Zwissler, O. El Bounkari, J. Bernhagen, Studying the pro-migratory effects of MIF. *Methods Mol. Biol.* **2080**, 1–18 (2020).
70. R. Windisch, A. Danese, A. Fischer, C. Wichmann, Data from "Engineering an inducible leukemia-associated fusion protein enables large-scale ex vivo production of functional human phagocytes". Gene Expression Omnibus. https://www.ncbi.nlm.nih.gov/geo/query/acc.cgi?acc=GSE237826. Deposited 20 July 2023.
71. R. Windisch, A. Danese, A. Fischer, C. Wichmann, Data from "Engineering an inducible leukemia-associated fusion protein enables large-scale ex vivo production of functional human phagocytes". Zenodo. https://zenodo.org/records/10521618. Deposited 1 August 2023.
72. A. Fischer, A. Danese, "reproducibility_Windisch_2023_sc". GitHub. https://github.com/DaneseAnna/reproducibility_Windisch_2023_sc. Deposited 10 July 2023.